American Mineralogist, Volume 92, pages 1616–1623, 2007

High-pressure optical spectroscopy and X-ray diffraction studies on synthetic cobalt aluminum silicate garnet

MICHAIL N. TARAN,[1,*] FABRIZIO NESTOLA,[2] HARUO OHASHI,[3] MONIKA KOCH-MÜLLER,[4] TONCI BALIC-ZUNIC,[5] AND LARS ARNSKOV OLSEN[5]

[1]Institute of Geochemistry, Mineralogy and Ore Formation, National Academy of Sciences of Ukraine, Paladin Avenue 34, 03680 Kyiv-142, Ukraine
[2]Dipartimento di Geoscienze, Università di Padova, Corso Garibaldi 37, I-35137 Padova, Italy
[3] HASHI Institute for Silicate Science, Nishinakanobu 1-9-25, Shinagawa, Tokyo 142-0054, Japan
[4]GeoForschungsZentrum, Sektion 4.1, Telegrafenberg, 14473 Potsdam, Germany
[5]Geological Institute, University of Copenhagen, Øster Voldgade 10, 1350 Copenhagen K, Denmark

ABSTRACT

The pressure-induced behavior of spin-allowed *dd*-bands of $^{VIII}Co^{2+}$ in the absorption spectra of synthetic $Co_3Al_2Si_3O_{12}$ garnet was studied from 10^{-4} to 13 GPa. The plots of the peak energy vs. pressure for the three sharpest well resolved bands at ca. 5160, 17 680, and 18 740 cm^{-1} display small but discernible breaks in linear relations between 4 and 5 GPa. Data from single-crystal X-ray diffraction likewise show discontinuities in trends of CoO_8 polyhedral volume and distortion, and Co-O and Si-O bond distances over this pressure range. These effects are related to a pressure-induced phase transition from the β- to α-isostructural polymorph of $Co_3Al_2Si_3O_{12}$.

Keywords: High-pressure optical spectroscopy, high-pressure X-ray diffraction, cobalt-bearing garnet, phase transitions

INTRODUCTION

$Co_3Al_2Si_3O_{12}$ garnet crystallizes in two isostructural polymorphs, the Co(α)- and Co(β)-forms showing space group $Ia\bar{3}d$. The in-situ transformation between the Co(α)- and Co(β)-forms has never been observed, therefore, the thermodynamic behavior of the phase transition is not known. Their structures differ slightly, as shown for example in ratios of the shared octahedral dodecahedral edge to the shared dodecahedral-dodecahedral edge distances. The unit-cell volume of the α-form measured at ambient conditions is slightly lower than that of the β-form (1503.07 and 1505.18 $Å^3$, respectively). Some crystal structure differences are shown for the atomic coordinates of the oxygen atom (Ohashi et al. 1981, 1995). The stability fields of the two phases are dependent on pressure, with the β-form being the low-pressure phase (Ohashi et al. 1981, 1995).

The crystal structure of garnet can be described in terms of isolated ZO_4 tetrahedra sharing corners with YO_6 octahedra, thereby forming a three-dimensional network in which cavities constituting eightfold-coordinated dodecahedra, XO_8, are located (see e.g., Armbruster and Geiger 1993; Merli et al. 1995; Geiger and Armbruster 1999). In $Co_3Al_2Si_3O_{12}$ garnet the Z, Y, and X sites are occupied by Si, Al, and Co^{2+}, respectively. Electronic *dd*-transitions of $^{VIII}Co^{2+}$ (d^7-configuration) cause a spectacular red color and several intense optical absorption bands in the visible and near infrared range in Co-bearing garnets (Ross et al. 1996; Geiger et al. 2000; Taran et al. 2002). As proposed theoretically (Milman et al. 2001) and established experimentally (Taran et al. 2002), the energies of the $^{VIII}Co^{2+}$ bands increase with pressure due to shortening of the Co-O distances.

Pressure-induced phase transitions in $3d^N$-ion bearing crystals are marked in absorption spectra as discontinuities in the energies of the absorption bands (e.g., Ross and Sowerby 1999). As the X-ray diffraction measurements at high pressure have reached an excellent level of accuracy, allowing determination of reliable crystal-structure data (e.g., Nestola et al. 2004 and references therein), it is possible to investigate even the small geometrical changes in crystal structures and relate them to the spectroscopically registered phase transitions. The aim of the present work is to determine by means of optical absorption spectroscopy and X-ray diffraction whether the isostructural Co(β)- to Co(α)-garnet phase transition can be induced by hydrostatic compression of Co(β)-garnet at room temperature.

EXPERIMENTAL DETAILS

The garnet single crystals were grown by the hydrothermal method using a belt type high-pressure apparatus (Fukunaga et al. 1979). The starting material was a mixture of 3CoO, Al_2O_3, and $3SiO_2$. The mixture, wetted by H_2O, was heated at 900 °C and 5 GPa for 3 h. The run product contained dark red isometric garnet grains ca. 0.1–0.2 mm in diameter and some other materials (Ohashi et al. 1981). Most garnet crystals contain numerous black inclusions of 10–30 μm size. Prepared as polished thin plates the samples are highly transparent and display a deep purple color, whereas the inclusions acquire a very dark blue color.

The high-pressure spectroscopic measurements in the UV-VIS-NIR were carried out on a thin, inclusion-free self-supporting garnet plate polished on both sides. Initially, the plate was of 55 μm thickness, allowing measurement of relatively weak *e*- and *f*-bands of Co^{2+} (see below), but still too thick to measure the more intense *g*-band which, in addition, significantly increases with pressure. The first set of high-pressure spectroscopic measurements was obtained on such

* E-mail: taran@igmr.relc.com

a sample in the range 10 000 to ca. 19 000 cm^{-1}, covering *e*- and *f*-bands only. The second set was obtained on the same garnet plate, but subsequently thinned to ca. 30 μm. On this sample the spectra were measured in the range 28 500 to 10 000 cm^{-1} covering the entire *e* to *g* band system.

The NUV-VIS-NIR high-pressure spectra (up to ~9.8 GPa) were recorded with a single-beam microspectrophotometer, which consisted of a SpectraPro-275 triple grating monochromator connected to a highly modified MIN-8 polarizing microscope and controlled by a PC. The spectra were scanned with steps $\Delta\lambda = 1$ nm in the range 350–450 nm (ca. 28 500–22 222 cm^{-1}) and $\Delta\lambda = 2$ nm in the range 420–1000 nm (ca. 22 222–10 000 cm^{-1}). To generate hydrostatic pressure up to ~10 GPa, the diamond-anvil cell (DAC) technique was used as described elsewhere (e.g., Langer et al. 1997).

High-pressure NIR spectra (up to ~13 GPa) in the range 11 000–4000 cm^{-1} were recorded on the thinned sample (see above) on a Bruker IFS 66v FTIR spectrometer. The spectrometer was equipped with a tungsten light source, a NIR/Quartz beam-splitter and a Hyperion microscope using Cassegrainian objectives and an InSb detector. The spectra were taken with an aperture size of 50 × 50 μm and a resolution of 2 cm^{-1}. For each spot the spectrum was averaged from 256 scans. The polished garnet plate and two ruby chips were embedded in the gasket hole (diameter of 300 μm) with a methanol-ethanol 4:1 mixture as a pressure-transmitting medium. Pressures measured on each ruby chip did not differ by more than 0.005 GPa, thus indicating nearly hydrostatic pressure conditions.

Several single crystals of $Co_3Al_2Si_3O_{12}$ were studied by X-ray diffraction at ambient conditions. The consistency of the unit-cell edge of all the samples tested indicates chemical homogeneity. Finally, based on its sharp optical extinction, absence of twinning and inclusions, a single crystal (size: $100 \times 70 \times 40$ μm^3) was selected for the high-pressure diffraction measurement. The sample was loaded in an ETH type DAC (e.g., Miletich et al. 2000). The diameters of diamond culets were 600 μm and a T301 gasket preindented to 75 μm, with a hole of 250 μm in diameter, was used. A mixture of methanol:ethanol:water with a ratio 16:3:1 was used as a pressure-transmitting medium. Together with the garnet sample, a single crystal of quartz as internal pressure standard (Angel et al. 1997) was loaded into the DAC.

X-ray intensity data were collected from a series of exposures on a CCD-equipped (Smart 1000) Bruker-AXS four-circle diffractometer utilizing graphite-monochromatized Mo$K\alpha$ radiation. A single 1 atm and 9 high-pressure data sets up to 7.4 GPa, each consisting of 1800 exposures, 0.2° ω-rotation apart and covering the accessible angular range up to $\sin\theta/\lambda = 0.68$, were collected at 298 K. The data collection strategy with runs of 20° rotation with adjustments of the 2θ angle for each run avoided the appearance of regions shaded by the DAC body on the detector's area, thus eliminating reflections with false zero intensity from integration. For intensity integration, data reduction and correction the Bruker-AXS software (SAINT+ and SADABS), which utilizes a three-dimensional extraction of intensities and the method of spherical harmonics for empirical absorption correction, was used. Final unit-cell edge at each pressure was obtained from a least-squares refinement of the positions of 450 to 480 reflections with $I > 10\sigma_I$ obtained through the integration process. The crystal structure parameters were also refined (space group $Ia\bar{3}d$) by a least-squares procedure using the SHELXL program (Sheldrick 1997), starting from the atomic coordinates of the ambient conditions data from Ohashi et al. (1995) and Dubrovinsky et al. (2006) who studied a crystal from the same synthesis run from which we selected the sample in this work. X-ray scattering factors for neutral atoms were taken from the *International Tables for Crystallography* (Wilson 1995). No violations of symmetry were found throughout the pressure range investigated. Thus the probability of multiple reflections (Umweganregung, Renninger effect) influencing the intensity data is considered low. Refinement details and crystal data of the ambient- and high-pressure measurements are reported in Table 1. Our atomic coordinates at room pressure obtained from the crystal in the DAC are in good agreement with those of Ohashi et al. (1995) and Dubrovinsky et al. (2006).

Results and discussion

Absorption spectra of the garnet plate of ~30 μm thickness and of a blue inclusion, measured at ambient conditions in the range 29 000–10 000 cm^{-1}, are shown in Figure 1a. As seen from this figure, the garnet spectrum is similar to those described by Ross et al. (1996), Geiger et al. (2000), and Taran et al. (2002). It consists of four partly overlapping bands labeled, in accordance with Taran et al. (2002), *e* to *h* with the peak energies typical for the Co-Al-silicate garnet. The bands *f*, *g*, and *h* are attributed

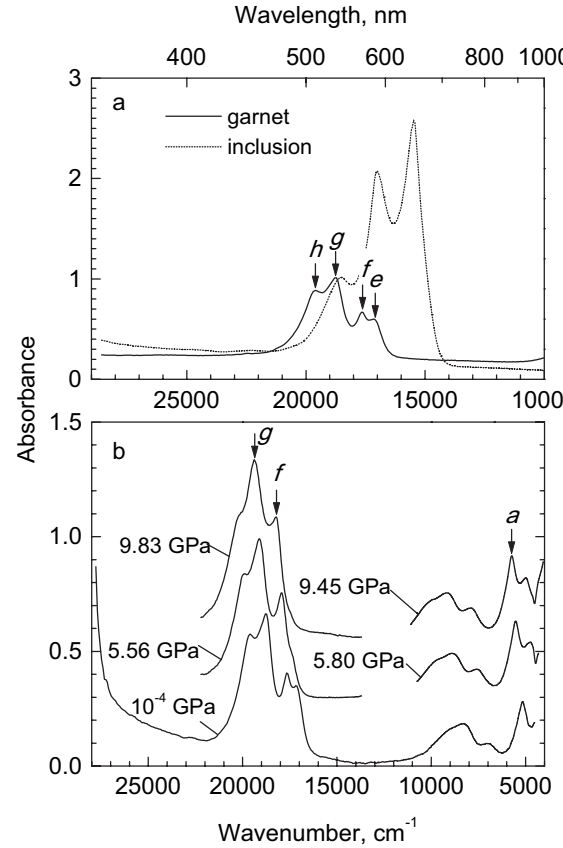

Figure 1. (**a**) Optical absorption spectra of synthetic $Co_3Al_2Si_3O_{12}$ garnet and dark blue inclusion at ambient pressure. (**b**) Optical absorption spectra of $Co_3Al_2Si_3O_{12}$ garnet at different pressures. For the sake of clarity, the spectra are shifted along the ordinate axis.

to the split electronic spin-allowed $^4A_2(^4F) \rightarrow {}^4T_1(^4P)$ transition of $^{VIII}Co^{2+}$ (d^7-configuration), while the *e*-band is believed to be caused by the spin-forbidden transition $^4A_{2g} \rightarrow {}^2T_{1g}(^2D)$ (Taran et al. 2002).

Examination under a polarizing microscope indicates that the inclusion material (as well as the host garnet) is optically isotropic. A SEM investigation shows that these inclusions consist of at least three phases of different SiO_2, Al_2O_3, and CoO contents. One phase of ca. $SiO_2 = 26.22$, $Al_2O_3 = 50.02$, and CoO = 23.54 wt% composition is strongly dominant (up to ca. 90 vol% of the inclusions), whereas the two others (6.73, 87.13, 5.78 and 14.16, 60.63, 24.76 wt% of SiO_2, Al_2O_3, and CoO, respectively) are present in much smaller amounts. Using Raman spectroscopy, we could not relate them to any known crystal phases. They are most likely glassy phases of different compositions.

The inclusion spectrum (Fig. 1a) consists of three intense partly overlapping bands with maxima at 15 480, 17 050, and 18 500 cm^{-1}. The barycenter of the bands is 17 010, which is close to ~16 960 cm^{-1} in the spectrum of a natural cobalt-bearing s.s.-spinel (Rossman 2006) where Co^{2+} enters the tetrahedral site (Burns 1993). Based on this observation, one may assume that Co^{2+} in the inclusion matrix also occupies tetrahedrally coordinated positions and the three bands in question are caused by the split $^4A_2(^4F) \rightarrow {}^4T_1(^4P)$ transition of $^{IV}Co^{2+}$. In accordance

TABLE 1. Crystal structure refinement details, unit-cell parameter a (Å), **unit-cell volume** V_0 (Å^3), **oxygen atomic coordinates** (x_O, y_O, z_O), isotropic displacement parameters (Å^2), **bond distances (Å), and polyhedral volumes** (Å^3) of $Co_3Al_2Si_3O_{12}$ garnet at different pressures

P (GPa)	10^{-4}	1.80	2.78	2.99*	4.77	4.84†	6.55*	7.01*	7.25*	7.40
$R_{4\sigma}$ (%)	5.6	5.1	4.1	3.4	4.2	3.9	3.6	4.5	3.7	3.9
GooF	1.2	1.0	1.1	0.9	1.0	0.9	1.0	1.0	0.9	1.0
Unique refl.	154	145	152	155	152	160	157	154	155	155
Parameters	9	9	9	9	9	9	9	9	9	9
$2\theta_{max}$ (°)	58.2	58.3	57.4	57.5	57.7	58.5	57.8	57.9	57.9	57.9
Crystal structure data										
a (Å)	11.4586(4)	11.4264(3)	11.4063(3)	11.3956(3)	11.3692(3)	11.3660(4)	11.3351(3)	11.3262(3)	11.3255(3)	11.3200(4)
V_0 (Å^3)	1504.5(1)	1491.9(1)	1484.0(1)	1479.8(1)	1469.6(1)	1468.3(1)	1456.4(1)	1452.9(1)	1452.7(1)	1450.6(1)
x_O	0.0338(5)	0.0339(5)	0.0337(4)	0.0333(4)	0.0335(4)	0.0336(4)	0.0334(4)	0.0333(5)	0.0330(4)	0.0330(4)
y_O	0.0506(5)	0.0509(5)	0.0519(4)	0.0514(4)	0.05272(4)	0.0516(4)	0.0526(5)	0.0526(5)	0.0527(4)	0.0529(4)
z_O	0.6528(5)	0.6529(4)	0.6525(4)	0.6525(4)	0.6523(4)	0.6528(4)	0.6527(4)	0.6524(4)	0.6522(4)	0.6528(4)
U_{iso} (Å^2) (Co)	0.0112(9)	0.0060(8)	0.0086(8)	0.0091(6)	0.0089(7)	0.0097(7)	0.0092(7)	0.0083(8)	0.0078(7)	0.0089(7)
U_{iso} (Å^2) (Al)	0.0056(11)	0.0062(13)	0.0052(10)	0.0040(8)	0.0041(10)	0.0059(10)	0.0051(11)	0.0049(11)	0.0040(10)	0.0042(10)
U_{iso} (Å^2) (Si)	0.0057(11)	0.0093(11)	0.0064(10)	0.0068(8)	0.0074(9)	0.0067(9)	0.0064(9)	0.0062(10)	0.0054(9)	0.0074(9)
(Si-O) (Å)	4×1.633(6)	4×1.629(5)	4×1.634(5)	4×1.634(4)	4×1.636(5)	4×1.626(4)	4×1.628(5)	4×1.630(5)	4×1.634(5)	4×1.629(5)
(Al-O) (Å)	6×1.885(6)	6×1.882(5)	6×1.877(5)	6×1.873(4)	6×1.871(5)	6×1.873(4)	6×1.869(4)	6×1.864(5)	6×1.861(4)	6×1.868(5)
$(Co-O)_{short}$ (Å)	4×2.211(6)	4×2.206(5)	4×2.205(5)	4×2.198(4)	4×2.201(5)	4×2.194(5)	4×2.190(5)	4×2.189(6)	4×2.188(5)	4×2.183(5)
$(Co-O)_{long}$ (Å)	4×2.339(6)	4×2.330(6)	4×2.314(5)	4×2.316(4)	4×2.296(5)	4×2.309(5)	4×2.291(5)	4×2.289(6)	4×2.286(5)	4×2.284(5)
V_z (Å^3)	2.20(2)	2.19(2)	2.20(2)	2.20(1)	2.21(1)	2.17(1)	2.18(1)	2.18(1)	2.20(1)	2.18(1)
V_y (Å^3)	8.92(5)	8.87(5)	8.80(4)	8.74(3)	8.72(4)	8.74(3)	8.68(4)	8.61(4)	8.57(4)	8.67(4)
V_x (Å^3)	20.19(10)	19.94(11)	19.73(9)	19.69(70)	19.40(8)	19.54(8)	19.22(8)	19.17(8)	19.12(8)	19.06(8)

* Data measured during decompression.
† Data measured during the second compression.

with crystal field theory (e.g., Bersuker 1996), their energies are noticeably lower than those of the *f*-, *g*-, and *h*-bands caused by the $^4A_{2g} \rightarrow {}^4T_{1g}(^4P)$ transition of Co^{2+} in eightfold coordination of the garnet structure. A relatively large splitting of the excited $^4T_1$ level is, almost certainly, caused by distortion of the tetrahedral site in the inclusion matrix. This deduction follows from comparison with the Co-bearing spinel, where the tetrahedral site is regular (e.g., Yamanaka and Takéuchi 1983) and the respective splitting of the excited $^4T_1$ level is much weaker (cf. Rossman 2006).

The high-pressure garnet spectra are shown in Figure 1b. The pressure dependency of the peak energies of the three sharpest and distinct bands of $^{VIII}Co^{2+}$, *a*, *f*, and *g*, were used to trace an apparent phase transition. The bands shift to higher energies with increasing pressure (Table 2) and all of them, except *e*-band, increase in intensity. Band *e* gradually diminishes and almost disappears somewhere between 4 and 5 GPa. These observations agree well with earlier results by Taran et al. (2002).

The plots of the energies of the *a*-, *f*-, and *g*-bands vs. pressure are shown in Figures 2a, 2b, and 2c, respectively. All three relations show deviations from linearity, which are seen as weak breaks in the pressure range from ca. 4 to 5 GPa. As a result, the data can best be fitted by two linear trends with a change in slope between 4 and 5 GPa.

The pressure-induced shifts of the electronic *dd*-bands of Co^{2+} in the spectra of $Co_3Al_2Si_3O_{12}$ garnet are undoubtedly caused by shortening of Co-O distances in CoO_8 dodecahedra during hydrostatic compression of the garnet structure. As a rule, such relations are smooth and close to linear (e.g., Langer et al. 1997). However, in the case of the pressure-induced phase transition or change of compression mechanism of a $3d^N$-ion-centered polyhedron there may be some discontinuities (e.g., Ross and Sowerby 1999) or breaks in the linear relations (Taran and Langer 2003).

The breaks in the three trends in Figure 2 are much weaker than the singularities observed at the $P2_1/c \rightarrow C2/c$ phase transition in clinoferrosilite or the change of the compression mechanism of Fe^{2+}(M2)-centered octahedra in orthopyroxenes

TABLE 2. Peak positions (cm^{-1}) of the *a*-, *f*-, and *g*-bands in the absorption spectra of synthetic $Co_3Al_2Si_3O_{12}$ garnet measured at different pressures, P (GPa)

a-band		*f*-band*		*g*-band	
P	Peak position	P	Peak position	P	Peak position
0.0001	5166	0.0001	17646	0.06	18767
0.15	5149	0.06	17639	0.55	18787
2.30	5314	0.55	17667	2.17	18886
3.83	5413	0.62	17671	2.96	18932
4.43	5430	1.85	17733	4.20	19025
5.00	5479	2.17	17743	5.56	19127
5.59	5513	2.76	17781	6.56	19174
5.80	5527	2.96	17784	7.18	19202
7.90	5661	3.83	17828	8.05	19266
9.47	5744	4.20	17861	8.18	19270
13.00	5923	4.77	17899	9.18	19332
		5.56	17938	9.83	19382
		5.93	17966		
		6.56	17992		
		6.73	18014		
		7.18	18028		
		8.05	18081		
		9.18	18152		
		9.83	**18221**		

Note: The band positions have been taken on maxima of the bands using the "Data Reading" option of Origin 5.0 software.
* Because the peak positions of the *f*-band were measured in two high-pressure experiments, on the "thick" and the "thin" sample (see text), the number of data for this band are larger than for the *g*-band, measured only on the "thin" sample.

(Ross and Sowerby 1999; Taran and Langer 2003, respectively). The trends can be fitted by single linear regressions with high correlation coefficients, $r = 0.9978$, 0.9992, and 0.9978, for the *a*-, *f*-, and *g*-bands, respectively (Fig. 2). Nevertheless, because the data for each band can be better fitted by two linear trends with a change in slope between 4 and 5 GPa, we presume that the observed breaks really exist and record a change of the CoO_8-polyhedral compressibility due to the β- to α-phase transition in the pressure range of 4 to 5 GPa. The weakness of the effect may be explained by very small differences between the structures of the two polymorphs (cf. Ohashi et al. 1995).

The *e*-band practically disappears at pressures from 4 to 5

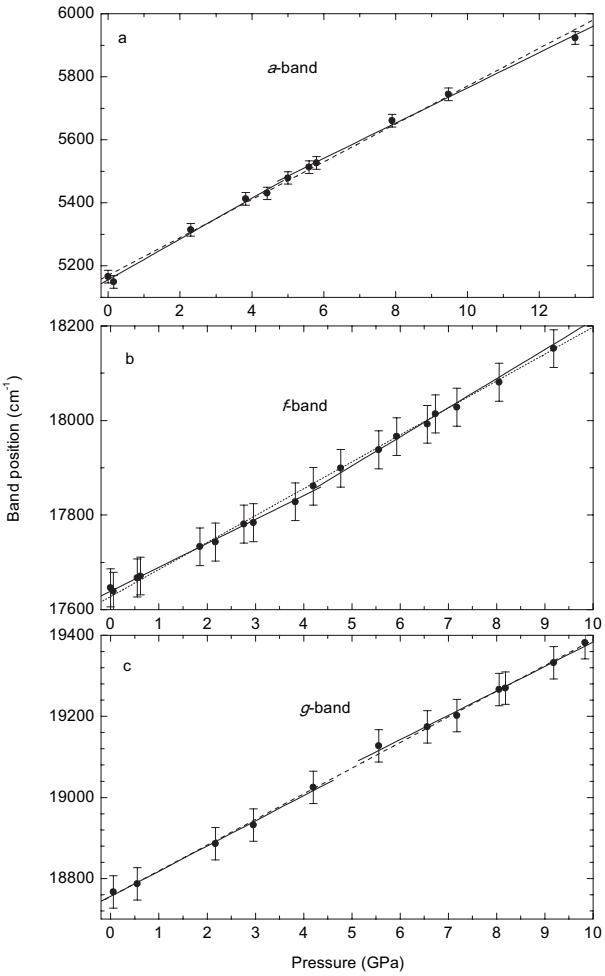

FIGURE 2. Peak position vs. pressure of the three sharpest prominent bands of Co^{2+} of $Co_3Al_2Si_3O_{12}$ garnet, *a*, *f*, and *g*. The solid lines are separate linear fits to data below and above 4.7 GPa, respectively. The dashed lines are linear fits to all data.

GPa, i.e., in the range where, presumably, the phase transition from Co(β)- to Co(α)-garnet takes place. As seen in Figure 1b, at 5.56 GPa the *e*-band is seen as a weak shoulder on the low-energy wing of the *f*-band. Taran et al. (2002) proposed that such behavior of the *e*-band may be due to the fact that, contrary to the spin-allowed bands *f*, *g*, and *h*, which increase in intensity with pressure (Fig. 1b), the *e*-band is caused by the spin-forbidden *dd*-transition, $^4A_{2g} \rightarrow {}^2T_{1g}(^2D)$, of $^{VIII}Co^{2+}$. Although the real mechanism of the band's behavior is still not completely understood, one may reasonably assume that it can be related to the β → α phase transition.

The above assumptions about the isostructural pressure-induced phase transition, revealed by optical absorption spectroscopy, are in good agreement with results of the high-pressure X-ray diffraction study of $Co_3Al_2Si_3O_{12}$ garnet (see below).

Equation of State

The equation of state (EoS) of $Co_3Al_2Si_3O_{12}$ was determined by fitting the volume-pressure data using a second-order Birch-Murnaghan EoS (Birch 1947) and the EOSFIT 5.2 program (Angel 2002). We obtained a bulk modulus K_{T0} = 190(2) GPa that is in good agreement with previous studies on garnets (see below). The unit-cell volume at zero pressure V_0 and the first pressure derivative K' were not refined (K' fixed to 4). Using different EoS (e.g., Murnaghan 1937) gave the same result within one standard deviation in K_{T0}.

Fixing K' to 4 for the equation of state used is justified by the linear behavior of volume vs. pressure for our sample (Fig. 3) and by previous single-crystal X-ray diffraction studies on garnets (Zhang et al. 1999) for which K' ranged between 4.2 and 4.4. The value of K_{T0} for the $Co_3Al_2Si_3O_{12}$ garnet is in good agreement with those of spessartine [K_{T0} = 189(1) GPa, $Mn_3Al_2Si_3O_{12}$] and almandine [K_{T0} = 185(3) GPa, $Fe_3Al_2Si_3O_{12}$] (Zhang et al. 1999), which show similar cationic radii for the M^{2+} metal ($^{VIII}Mn^{2+}$ = 0.96 Å, $^{VIII}Fe^{2+}$ = 0.92 Å, $^{VIII}Co^{2+}$ = 0.90 Å, based on Shannon 1976). In contrast, even though Mg in pyrope, $Mg_3Al_2Si_3O_{12}$, has a cationic radius of 0.89 Å (very close to that of Co) this mineral shows a lower bulk modulus (K_{T0} = 171 GPa) due to the different electronic configuration of Mg^{2+} with respect to that of the $3d^N$ transition-metal ions (Zhang et al. 1999). Such a difference has been observed also for spinels, carbonates, olivine, and clinopyroxenes (Hazen 1993; Zhang and Reeder 1997; Zhang 1998; Nestola et al. 2005).

From Figure 3, and based on the full range of data, it can be seen that a weak deviation from a common linear trend exists in the present case. If only the data below 4 GPa are used in the linear fit, the observed volumes at higher pressures lie above the predicted trend. The decrease in volume between ambient pressure and 7.4 GPa is 3.6%, whereas the one predicted from the fit to the data before the β → α phase transition would be 3.9%. As the deviation is small, confirmation from the other structural parameters about the change in properties during this transition is needed. The calculated bulk modulus was obtained by fitting the full range of data, and should represent an averaged value for the low- and high-pressure modifications of $Co_3Al_2Si_3O_{12}$. If our conclusion about the change in trends in volume compression at the phase transition is correct, the high-pressure phase has a slightly larger bulk modulus than the low-pressure one.

Crystal structure evolution at high pressure

Analysis of the polyhedral volumes as a function of pressure gives an indication about the structural compression mechanisms. The pressure relations of SiO_4-, AlO_6-, and CoO_8-polyhedral volumes are shown in Figure 4. As seen from the figure, in spite of a relatively large uncertainty in Si-O bond lengths, the SiO_4-tetrahedral volumes seem to show two trends with a discontinuous decrease at ~4.8 GPa pressure. The step-wise decrease in volume may be due to a discontinuous Si-O bond shortening at the β to α phase transition. The Si-O distance changes from 1.636(5) Å at 4.77 GPa to 1.626(4) Å at 4.84 GPa. Note that these Si-O distances are consistent with those reported by Ohashi et al. (1995): 1.634(1) and 1.627(2) Å for the β- and α-$Co_3Al_2Si_3O_{12}$ garnets, respectively.

The AlO_6-octahedral volume decreases with pressure with a contraction by about 2.8%. The CoO_8-dodecahedon displays the highest compressibility among the three polyhedra: its volume decreases by 5.6% in the pressure range 1×10^{-4} to 7.4 GPa. This

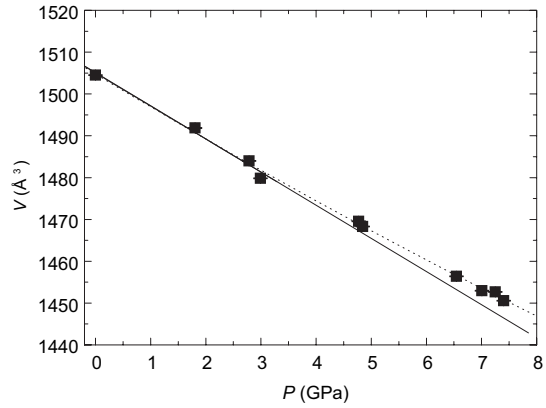

FIGURE 3. Plot of the unit-cell volume of $Co_3Al_2Si_3O_{12}$ garnet vs. pressure. The solid line is a linear fit to data below 4 GPa. The dotted line is a linear fit to all data.

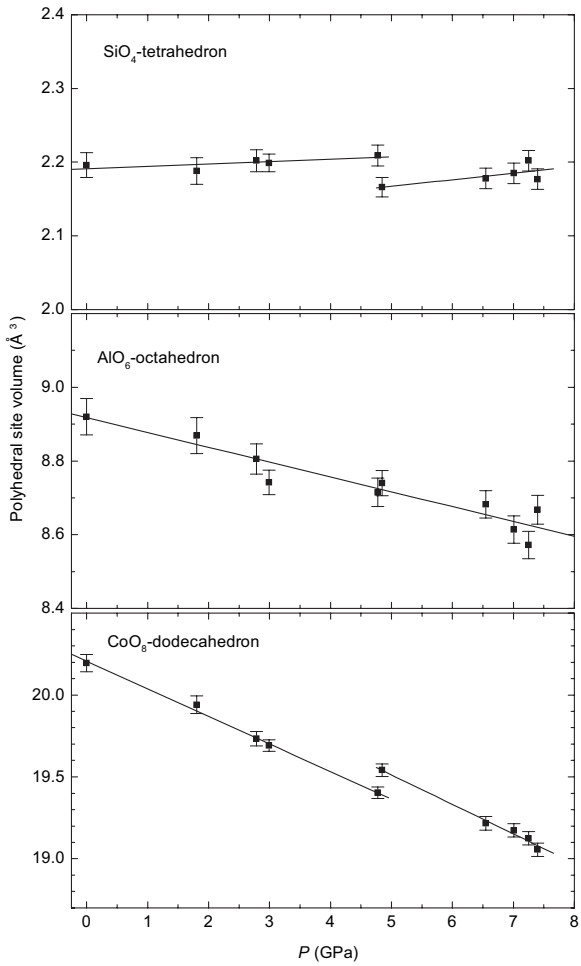

FIGURE 4. Plots of the polyhedral site volume of three structural units, SiO_4 tetrahedron, AlO_6 octahedron, and CoO_8 dodecahedron, in the structure of $Co_3Al_2Si_3O_{12}$ garnet vs. pressure. The solid straight lines are linear fits to data. Jumps in the SiO_4 and CoO_8 polyhedral volumes vs. pressure probably indicate a phase transition from the β- to α-polymorph in $Co_3Al_2Si_3O_{12}$ garnet.

is consistent with the "blue" shifts of the absorption bands with increasing pressure (Fig. 2). As seen from Figure 4, the CoO_8-polyhedral volume vs. pressure plot displays two trends with a jump at ~4.8 GPa. We believe that this discontinuity is related to the breaks between 4 and 5 GPa seen in the linear trends of the *a*, *f*, and *g* absorption bands (Fig. 2) and indicates the β to α phase transition in $Co_3Al_2Si_3O_{12}$.

The octahedron and the tetrahedron in the garnet structure have a single Al-O and Si-O bond distance, whereas the large and more distorted CoO_8-polyhedron shows two independent bond distances: $4 \times (Co\text{-}O)_{long}$ and $4 \times (Co\text{-}O)_{short}$. If we plot the short and long Co-O bond distances as a function of pressure (Fig. 5), it is easy to see that the observed discontinuity in CoO_8-polyhedral volume is mainly due to the evolution of $(Co\text{-}O)_{long}$. This confirms the $\beta \rightarrow \alpha$ phase transition in $Co_3Al_2Si_3O_{12}$ garnet at around 4.8 GPa (cf. Figs. 5 and 6).

Distortions of the SiO_4, AlO_6, and CoO_8 polyhedra vs. pressure were calculated using IVTON software (Balic-Zunic and Vickovic 1996). Due to single bond distances, only volume distortions (deviations from the regular tetrahedron or regular octahedron, which give the maximum volume with the same bond distance) are present in the SiO_4-tetrahedron, and AlO_6-octahedron (Fig. 6a). They show very low variations of 1.6–1.8% and 0.2–0.3%, respectively. Volume distortion of SiO_4 remains nearly constant; that of AlO_6 displays a weakly increasing trend. Note that with increasing pressure the AlO_6 octahedron in pyrope, for instance, also becomes more distorted, whereas the SiO_4 tetrahedron becomes more regular (Zhang et al. 1998).

Besides the volume distortion, an asphericity distortion is intrinsic for the CoO_8-dodecahedron (Balic-Zunic and Makovicky 1996); this is due to the deviation of ligands from a sphere fitted to the coordination polyhedron (because of the two different bond distances). The volume distortion and the asphericity of CoO_8 show diverging trends up to the phase transition; the former is increasing, whereas the latter is decreasing (Fig. 6b). The total distortion (which is the sum of the two) decreases as a consequence of the larger change in asphericity. Above 4.7 GPa the trends are opposite, again confirming a phase transi-

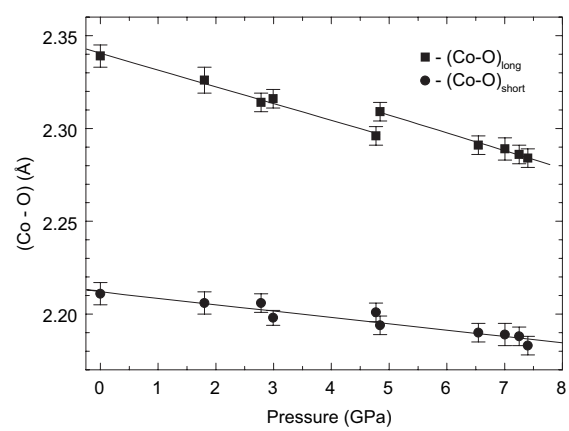

FIGURE 5. Plots of $(Co\text{-}O)_{short}$ and $(Co\text{-}O)_{long}$ distances vs. pressure. A distinct jump in the relation of $(Co\text{-}O)_{long}$ distance vs. pressure probably indicates phase transition from the β- to α-polymorph in $Co_3Al_2Si_3O_{12}$ garnet.

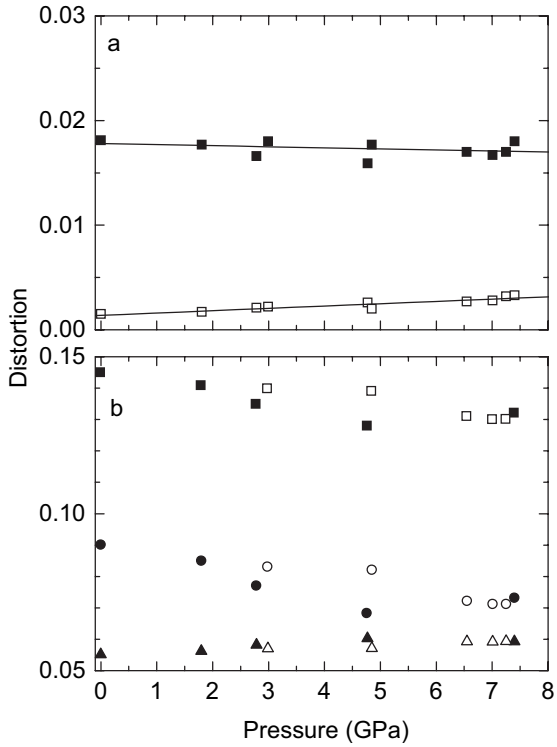

FIGURE 6. (**a**) Plots of the volume distortions of AlO_6 octahedron (empty squares) and SiO_4 tetrahedron (filled squares) in the structure of $Co_3Al_2Si_3O_{12}$ garnet vs. pressure. The solid straight lines are linear approximations. (**b**) Plots of the distortion parameters for the CoO_8 dodecahedron vs. pressure: Triangles = volume distortion, circles = asphericity, squares = total distortion. Filled symbols represent data on compression, empty = on decompression.

tion at approximately this pressure. The spread of data obtained during compression and decompression points to a hysteresis effect. Evidently, the structure remains fixed for some time in the α-modification during decompression at room temperature. The effect can also be observed to a minor extent in other properties such as Co-O distances and polyhedral volumes (Figs. 4 and 5). A note on the symmetry distortion of the polyhedron should be made at this point. The symmetry of the large cation dodecahedron in the structure of garnets is D_2 but its shape is close to a square antiprism with an ideal symmetry D_{4d}. In fact, the shape is transitional between an antiprism and a cube (symmetry O_h), being closer to the former. The approach to either of the latter two idealized symmetries must be accompanied by an equalization of bond lengths and decrease of the asphericity parameter. However, the volume distortion is calculated relative to the polyhedron, which has the highest volume capacity for the coordination number 8 and this is the bisdisphenoid with symmetry D_{2d}. Inside the frames used for calculation (and represented on Fig. 6), an ideal Archimedean antiprism would attain a volume "distortion" of 0.0535, whereas an ideal cube would attain 0.1522. In other words they have 5.35 and 15.22% less volume efficiency, respectively, than the ideal bisdisphenoid. An increase in the volume distortion of the dodecahedron above 0.0535 with increasing pressure means therefore that it changes its antiprismatic shape toward a cubic one. In the phase transformation from the β- to the α-form, the Co polyhedron shows both an increase in regularity connected with a reduced difference in bond distances (smaller asphericity) and a moderate distortion from a fully antiprismatic shape toward a cubic one.

It should be noted that the evolving geometry of the Co coordination polyhedron seemingly contradicts a pressure-induced intensification of the spin-allowed absorption bands of $^{VIII}Co^{2+}$ (see above). Theoretically, the intensity of spin-allowed *dd*-bands in spectra of $3d^N$-ion bearing crystals is related to the non-centrosymmetric character of the ligand surroundings (e.g., Bersuker 1996). However, the CoO_8-dodecahedron approaches a centrosymmetric configuration by becoming more spherical and with the geometry becoming closer to cubic under increasing pressure. The pressure-induced intensification of spin-allowed absorption bands $^{VIII}Co^{2+}$ in $Co_3Al_2Si_3O_{12}$ garnets with pressure was first reported by Taran et al. (2002) where it was explained by an increase of the spin-orbit coupling of $^{VIII}Co^{2+}$ upon compression. Probably, in Co-garnet this latter mechanism of the band's intensification predominates over the effect of band weakening caused by the decrease of the X-site distortion.

The splitting of the $^4T_1(^4P)$-level into three components *h*, *f*, and *g* may, at least partly, be due to the low symmetry of the X site, D_2, in the structure of silicate garnets. For this reason, it can be expected that the pressure-induced decrease of the X site distortion (Fig. 6) will lead to reduced splitting between the $^4A_2(^4F) \rightarrow {}^4T_1(^4P)$ transition components. Indeed, the splitting between the *g*- and *h*-band seems to decrease as the overlap between them clearly increases (Fig. 1b). It is not easy to trace this tendency over the whole pressure range since the increased overlapping of the bands strongly hampers the determination of the *h*-band peak position (Fig. 1b). Note that in this case the curve fitting procedure is not very useful as the results of the curve resolution are questionable, needing many more fitting components than seen by eye (Taran et al. 2002). In contrast to the *g*- and *h*-band splitting, the splitting between the much better separated *f*- and *g*-bands clearly increases, though only from ca. 1120 to 1160 cm^{-1}, in the pressure range 1×10^{-4} to 9.83 GPa (Table 2). It seems, however, that the plot of splitting vs. pressure has a smooth maximum between ca. 7 and 8 GPa (Fig. 7a). We do not exclude that such a change in the trend of the bands' separation, shown conditionally by two dashed straight lines in Figure 7a, can be related to the $\beta \rightarrow \alpha$ phase transition at around 5 GPa. A change in the pressure dependence of the *f*- and *g*-band splitting is also well seen from the plot of the peak energies of *f*- vs. *g*-band at different pressures (Fig. 7b). Indeed, *g*-band peak energy increases with an increase of *f*-band peak energy as two separate trends. Correlations of these two trends can be represented by two simple equations, $g = (1 + 0.19) f - 2141$ ($r = 0.9990$) and $g = (1 - 0.07) f + 2468$ ($r = 0.9978$) for the low-pressure β- and high-pressure α-polymorph, respectively. These correlations clearly show that the splitting between *f*- and *g*-bands increases relatively quickly with pressure in the low-pressure polymorph and decreases weakly with pressure in the high-pressure one.

The polyhedral modulus of the CoO_8 polyhedron, k^{BL}_{poly}, calculated from the bond-length (BL) data at $P_1 = 10^{-4}$ GPa and $P_2 = 7.4$ GPa[1] and using the expression

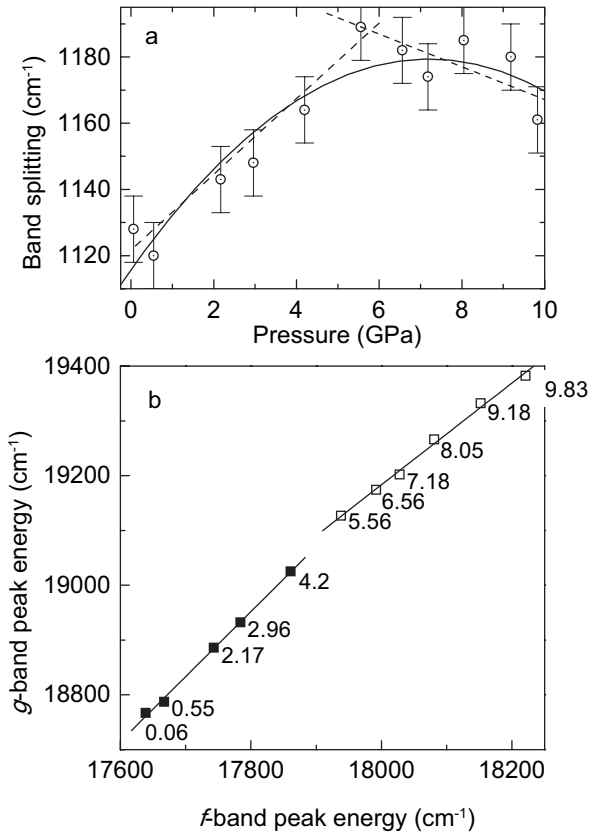

FIGURE 7. (**a**) Plot of the splitting between *f*- and *g*-absorption bands of $^{VIII}Co^{2+}$ vs. pressure. The relation, fitted by the polynomial regression $\delta = 1115 + 17.67 \cdot P - 1.227 \cdot P^2$ (solid line), displays a smooth maximum between 7 and 8 GPa, which may arise from the two trends (the dashed lines) before and after the β to α phase transition in $Co_3Al_2Si_3O_{12}$. (**b**) *g*-band peak energy plotted against *f*-band peak energy. Filled symbols represent the data points for the low-pressure polymorph, and open symbols represent the data points for the high-pressure polymorph.

$$\bar{\beta} = \frac{-2(\bar{R}_2 - \bar{R}_1)}{(\bar{R}_1 + \bar{R}_2)(P_2 - P_1)}$$

where $\bar{\beta}$ is the mean linear polyhedral compressibility, $\bar{R}_1$ and $\bar{R}_2$ are mean Co-O distances

$$(\bar{R} = \frac{R_{long} + R_{short}}{2})$$

measured at pressures P_1 and P_2, respectively (e.g., Hazen and Finger 1982) and

$$k_{poly}^{BL} = \frac{1}{3\bar{\beta}} \text{ (Langer 1990),}$$

is ~134 GPa. This value is appreciably lower than the bulk modulus, $K_{T0} = 190(2)$ GPa, indicating that the structural unit CoO_8 is more compressible than the whole structure of the $Co_3Al_2Si_3O_{12}$ garnet, as also seen from the change of its volume (5.6%) compared to the change of the unit-cell volume (3.6%).

The polyhedral modulus of AlO_6 calculated from Table 1 is 272 GPa. For comparison, the polyhedral moduli of the MgO_8 and AlO_6 polyhedra in pyrope are 107(1) and 211(11) GPa, respectively (Zhang et al. 1998), which indicates that in pyrope, $Mg_3Al_2Si_3O_{12}$, these structural units are significantly more compressible than in $Co_3Al_2Si_3O_{12}$.

The SiO_4 polyhedron does not show a measurable compressibility apart from the discontinuity at about 5 GPa, which was not observed in pyrope. A much broader pressure range, e.g., up to 33 GPa (Zhang et al. 1998), should be covered to detect noticeable changes in the SiO_4-polyhedral volume from which its bulk modulus can be determined.

The differences in compressibility of coordination polyhedra in Co-garnet and pyrope could be related to the different behavior of the minerals containing 3*d* transition metals. This seems to cause a general decrease in compressibility even when there are not significant differences in cationic radius with respect to the other elements (see Hazen 1993; Zhang and Reeder 1997; Zhang 1998; Nestola et al. 2005).

The polyhedral modulus of CoO_8 can also be evaluated from the pressure-induced shift of the *a*-band of $^{VIII}Co^{2+}$ in optical absorption spectra because, in theory, this band is caused by the $^4A_{2g} \rightarrow {}^4T_{2g}(^4F)$ transition of $^{VIII}Co^{2+}$ (Ross et al. 1996) whose energy, ν, is a function of the crystal field strength Dq, $\nu = 10Dq$. In turn, Dq depends on the mean Co-O distance $\bar{R}$ in the coordination dodecahedron as

$$Dq = \frac{3 < r^4 > (Z_L e^2)}{5\bar{R}^5}$$

where $<r^4>$ is the mean value of the fourth power of the 3*d*-electron radius, Z_L is effective ligand charge, and e is the charge of electron. Assuming that the numerator is nearly constant, values of $\bar{R} = <\text{Co-O}>$ at different pressures can be evaluated (cf. Langer 1990). The spectroscopic value of the polyhedral modulus of CoO_8, k_{poly}^{spectr}, obtained from the spectroscopic data measured at ambient pressure and at 7.9 GPa (Table 2), is ~145 GPa. It is in good agreement with the k_{poly}^{BL} value, ~134 GPa, obtained by BL calculations (see above).

ACKNOWLEDGMENTS

We are grateful to R. Spiess (Department of Geosciences of Padova) for SEM investigation of the inclusions in garnets. The high-pressure XRD measurements were financed by the Natural Science Council of Denmark. Comments from the associated editor E. Libowitzky and the referees C.A. Geiger and H. Keppler helped significantly in improving the text. We thank J. Bailey for the critical reading of the manuscript and language corrections.

REFERENCES CITED

Angel, R.J. (2002) EoS-Fit V5.2 program. Crystallography Laboratory, Virginia Tech, Blacksburg.

Angel, R.J., Allan, D.R., Milletich, R., and Finger, L.W. (1997) The use of quartz as an internal pressure standard in high-pressure crystallography. Journal of Applied Crystallography, 30, 461–466.

Armbruster, T. and Geiger, C.A. (1993) Andradite crystal-chemistry, dynamic X-site disorder and structural strain in silicate garnets. European Journal of Mineralogy, 5, 59–71.

Balic-Zunic, T. and Makovicky, E. (1996) Determination of the centroid or "the best center" of a coordination polyhedron. Acta Crystallographica, B52, 78–81.

Balic-Zunic, T. and Vickovic, I. (1996) IVTON—program for the calculation of geometrical aspects of crystal structures and some chemical applications.

[1]The discontinuity at around 5 GPa makes the calculation not quite correct. In fact, this procedure can provide only an indication of bulk modulus. To get the actual values one should separate the data below and above the discontinuity.

Journal of Applied Crystallography, 29, 305–306.
Bersuker, I.B. (1996) Electronic structure and properties of transition metal compounds: Introduction to the theory. Wiley-Interscience, New York.
Birch, F. (1947) Finite elastic strain of cubic crystals. Physical Review, 71, 809–824.
Burns, R.G. (1993) Mineralogical Applications of Crystal Field Theory, 2nd edition. Cambridge University Press, U.K.
Dubrovinsky, L., Dubrovinskaya, N., Kantor, I., Nestola, F., and Gatta, G.D. (2006) High-brilliance X-ray system for high-pressure in-house research: applications for studies of superhard materials. High-Pressure Research, 26, 137–143.
Fukunaga, O., Yamaoka, S., Endo, T., Akaishi, M., and Kanda, H. (1979) Modification of belt-like high-pressure apparatus. High-Pressure Science and Technology, 1, 846–852.
Geiger, C.A. and Armbruster, T. (1999) The crystal structure of a garnet solid solution $(Ca_{0.9}Mg_{0.1})_3Al_2[SiO_4]_3$ at 295 K and 100 K: Local site behavior—dynamic and static disorder. Zeitschrift für Kristallographie, 214, 211–215.
Geiger, C.A., Stahl, A., and Rossman, G.R. (2000) Single-crystal IR- and UV/VIS-spectroscopic measurements on transition-metal-bearing pyrope: the incorporation of hydroxide in garnet. European Journal of Mineralogy, 12, 259–271.
Hazen, R.M. (1993) Comparative compressibilities of silicate spinels: Anomalous behavior of $(Mg, Fe)_2SiO_4$. Science, 259, 206–209.
Hazen, R.M. and Finger, L.W. (1982) Comparative Crystal Chemistry. Temperature, pressure, composition and the variation of crystal structure. Wiley and Sons, Ltd., New York.
Langer, K. (1990) High pressure spectroscopy. In A. Mottana and F. Burragato, Eds., Absorption Spectroscopy in Mineralogy, p. 228–284. Elsevier, Amsterdam.
Langer, K., Taran, M.N., and Platonov, A.N. (1997) Compression moduli of Cr^{3+}-centered octahedra in a variety of oxygen-based rock-forming minerals. Physics and Chemistry of Minerals, 24, 109–114.
Merli, M., Callegari, A., Cannillo, E., Caucia, F., Leona, M., Oberti, R., and Ungaretti, L. (1995) Crystal-chemical complexity in natural garnets: structural constraints on chemical variability. European Journal of Mineralogy, 7, 1239–1249.
Miletich, R., Allan, D.R., and Kuhs, W.F. (2000) High-pressure single crystal techniques. In R.M. Hazen and R.T. Downs, Eds., High-temperature and high-pressure crystal chemistry, 41, p. 445–519. Reviews in Mineralogy and Geochemistry, Mineralogical Society of America, Chantilly, Virginia.
Milman, V., Akhmatskaya, E.V., Nobes, R.H., Winkler, B., Pickard, C.J., and White, J.A. (2001) Systematic ab initio study of the compressibility of silicate garnets. Acta Crystallographica, B57, 163–177.
Murnaghan, F.D. (1937) Finite deformations of an elastic solid. American Journal of Mathematics, 49, 235–260.
Nestola, F., Boffa Ballaran, T., and Tribaudino, M. (2004) High pressure behavior, transformation and crystal structure of synthetic iron-free pigeonite. American Mineralogist, 89, 189–196.
Nestola, F., Boffa Ballaran, T., Tribaudino, M., and Ohashi, H. (2005) Compressional behavior of $CaNiSi_2O_6$ clinopyroxene: bulk modulus systematic and cation type in clinopyroxenes. Physics and Chemistry of Minerals, 32, 222–227.
Ohashi, H., Fujita, T., and Osawa, T. (1981) Structure of $Co_3Al_2Si_3O_{12}$ garnet. Journal of the Japanese Association of Mineralogists, Petrologists and Economic Geologists, 76, 58–60.
Ohashi, H., Osawa, T., and Sato, A. (1995) Low-pressure polymorph of $Co_3Al_2Si_3O_{12}$. Acta Crystallographica, C51, 2213–2215.
Ross, C.R., Keppler, H., Canil, D., and O'Neill, H.St.C. (1996) Structure and crystal-field spectra of $Co_3Al_2(SiO_4)_3$ and $(Mg, Ni)_3Al_2(SiO_4)_3$ garnet. American Mineralogist, 81, 61–66.
Ross, N.L. and Sowerby, J.R. (1999) High-pressure crystal-field spectra of single-crystal clinoferrosilite. European Journal of Mineralogy, 11, 791-801.
Rossman, G.R. (2006) Mineral Spectroscopy Server, http://minerals.gps.caltech.edu. California Institute of Technology, Pasadena.
Shannon, R.D. (1976) Revised effective ionic radii and systematic studies of interatomic distances in halides and chalcogenides. Acta Crystallographica, A32, 751–757.
Sheldrick, G.M. (1997) SHELXL-97, a program for crystal structure refinement. University of Göttingen, Germany.
Taran, M.N. and Langer, K. (2003) Single-crystal high-pressure electronic absorption spectroscopic study of natural orthopyroxenes. European Journal of Mineralogy, 15, 689–695.
Taran, M.N., Langer, K., and Geiger, C.A. (2002) Single-crystal electronic absorption spectroscopy of synthetic chromium-, cobalt-, and vanadium-bearing pyropes at different temperatures and pressures. Physics and Chemistry of Minerals, 29, 362–368.
Yamanaka, T. and Takéuchi, Y. (1983) Ordering-disordering transition in $MgAl_2O_4$ spinel at high temperature up to 1700 °C. Zeitschrift für Kristallographie, 165, 65–78.
Zhang, L. (1998) Single crystal hydrostatic compression of $(Mg,Mn,Fe,Co)_2SiO_4$ olivines. Physics and Chemistry of Minerals, 25, 308–312.
Zhang, L. and Reeder, R.J. (1997) Comparative compressibilities of calcite-structure carbonates. EOS Transaction American Geophysical Union, 78, F752.
Zhang, L., Ahsbahs, H., and Kutoglu, A. (1998) Hydrostatic compression and crystal structure of pyrope to 33 GPa. Physics and Chemistry of Minerals, 25, 301–307.
Zhang, L., Ahsbahs, H., Kutoglu, A., and Geiger, C.A. (1999) Single-crystal hydrostatic compression of synthetic pyrope, almandine, spessartine, grossular and andradite garnets at high pressures. Physics and Chemistry of Minerals, 27, 52–58.
Wilson, A.J.C., Ed. (1995) International tables for crystallography, Vol. C. Kluwer Academic Publishers, Dordrecht, The Netherlands.

MANUSCRIPT RECEIVED SEPTEMBER 21, 2006
MANUSCRIPT ACCEPTED JUNE 3, 2007
MANUSCRIPT HANDLED BY EUGEN LIBOWITZKY